JOURNAL OF AIRCRAFT
Vol. 51, No. 1, January–February 2014

Model Reduction for Aeroservoelastic Systems

Claudia P. Moreno,* Peter J. Seiler,† and Gary J. Balas‡
University of Minnesota, Minneapolis, Minnesota 55455

DOI: 10.2514/1.C032341

A model-reduction method for linear, parameter-varying systems based on parameter-varying balanced realizations is proposed for a body freedom flutter vehicle. A high-order linear, parameter-varying model with hundreds of states describes the coupling between the short period and first bending mode with additional structural bending and torsion modes that couple with the rigid body dynamics. However, these high-order state–space models result in a challenging control design, and hence a reduced-order linear, parameter-varying model is desired. The objective is to reduce the model state order across the flight envelope while retaining a common set of states in the linear, parameter-varying model. A reduced-order linear, parameter-varying model with tens of states is obtained by combining classical model reduction and parameter-varying balanced realizations reduction techniques. The resulting reduced-order model captures the unstable dynamics of the vehicle and is well suited for the synthesis of active flutter suppression controllers.

Nomenclature

A	=	state matrix
B	=	input matrix
C	=	output state matrix
D	=	input feedthrough matrix
G	=	plant model
P	=	controllability Gramian
Q	=	observability Gramian
$\mathbb{R}$	=	set of real numbers
T	=	similarity transformation
u	=	input vector
X	=	control Riccati inequality solution
x	=	states vector
x_a	=	aerodynamic lag states vector
Y	=	filtering Riccati inequality solution
y	=	output vector
γ	=	fixed value of exogenous input
δ	=	control surface deflection
Λ	=	eigenvalues matrix
λ	=	system eigenvalues
ξ	=	generalized coordinates
ρ	=	exogenous input vector
Σ	=	singular values matrix
σ	=	system singular values

I. Introduction

THE need for improved performance and reduced operating costs has led modern aircraft designers to adopt lightweight, high-aspect-ratio flexible wings. Reducing weight decreases aerodynamic drag, leading to less fuel consumption. High-aspect-ratio wings minimize drag over lift, improving the aircraft performance on aspects such as long range and endurance. These modifications are being applied to modern commercial airplanes, mainly by using composite materials for both fuselage and wings. As result, the new generation of long-range airliners developed by Boeing (787) and Airbus (A350) show higher fuel efficiency and lower costs than previous similar sized aircraft.

The aerodynamic advantages of high-aspect-ratio flexible wings are also being exploited to develop autonomous aircraft for intelligence, surveillance, and reconnaissance missions. These lightweight, high-altitude, long-endurance vehicles with large wingspan exhibit high flexibility and significant deformation in flight, leading to increased interaction between the rigid body and structural dynamics modes. This phenomenon, called body freedom flutter (BFF), occurs as the aircraft rigid body frequency response increases with airspeed and interacts with a wing vibration mode, typically the wing bending mode. The interaction can lead to poor handling qualities and may result in dynamic instability. Hence, an integrated active approach to flight control, flutter suppression, and structural mode attenuation is required to meet the desired handling quality performance and gust load alleviation for modern flexible aircraft.

Numerous flutter-suppression control strategies have been proposed to address the coupled rigid body and aeroelastic dynamics. These include optimal control [1,2], dynamic inversion control [3], robust multivariable control [4], model predictive control [5], and gain scheduled control [6–9]. A majority of these strategies are model-based and, hence, require an accurate description of the aeroelastic behavior of the aircraft. Flutter analysis of aircraft has been widely studied [10–13], and numerous researchers have addressed aeroelastic modeling for highly flexible aircraft [1,3,9,14]. Currently, modeling of a flexible aircraft requires a geometric structural model coupled with a consistent aerodynamic model. The nonlinear aeroelastic models are derived based on structural finite elements and lifting-surface theory, both of which are available in general purpose commercial codes [15–17]. It is standard practice to represent the fully coupled nonlinear aircraft model as a linear model that varies as a function of parameters across the flight envelope, i.e., linear parameter-varying (LPV) systems; hence, the traditional description of aeroservoelastic (ASE) models for control fits naturally in the LPV framework.

The LPV system framework provides a rich, theoretical control analysis and design framework for nonlinear systems [7,18–24]. Unfortunately, the inclusion of structural dynamics and aeroelastic effects in modeling flexible aircraft results in linear, dynamic models with a large number of degrees of freedom. It is unrealistic to use these high-order models for control design because modern control methods will result in controllers with high-state-order models. Even more, practical implementation of high-order controllers is usually avoided because computational issues associated with synthesizing LPV controllers increase with the state order of the design model. Hence, a reduced-order LPV model of the flexible aircraft will

Presented as Paper 2012-4859 at the AIAA Atmospheric Flight Mechanics Conference, Minneapolis, MN, 13–16 August 2012; received 18 March 2013; revision received 31 May 2013; accepted for publication 14 June 2013; published online 22 January 2014.

*Graduate Research Assistant, Department of Aerospace Engineering and Mechanics. Student Member AIAA.

†Assistant Professor, Department of Aerospace Engineering and Mechanics. Member AIAA.

‡Professor and Department Head, Department of Aerospace Engineering and Mechanics. Member AIAA.

allow model-based, gain-scheduled multivariable controllers to be synthesized and implemented on ASE flight vehicles.

Several LPV model-reduction techniques including balanced truncation [25], projection methods based on linear matrix inequalities (LMIs) [26], and bounded parameter variation rates [27,28] have been proposed in the literature. However, often these methods introduce derivative terms with respect to time that make the reduction problem harder to solve. Additionally, ASE models are, in general, systems with mixed stability; therefore, approaches that require the system to be stable cannot be applied. LPV model-reduction methods that can accomodate unstable systems are formulated via a coprime factorization to find a balanced parameter varying system [27–30].

This paper describes the development of a low-order, control-oriented ASE model based on a combination of classical and LPV model-reduction techniques. Balanced reduction methods for LPV systems are combined with classical truncation and residualization approaches and applied to an experimental BFF test vehicle developed by Lockheed Martin Aeronautics for the U.S Air Force [31,32]. The truncation and residualization methods are performed on the full-order BFF model to obtain a reduced model with consistent states (i.e., the same state vector is defined across the flight envelope). Next, a balanced realization of the LPV system is obtained based on a quadratically stable right coprime factorization [29,30]. The states with small contribution to the input/output energy of the system, identified by the balanced realization, are eliminated by singular perturbation approximation resulting in an LPV reduced-order model that can be used to synthesize gain-scheduled controllers. Frequency domain comparisons are performed between the original and reduced-order BFF models.

The paper is organized as follows. Section II describes the LPV framework for ASE models. Section III presents an overview of model-reduction techniques reported in the literature. Section IV describes the BFF test vehicle, and the results for the approximation of LPV unstable systems are presented. Finally, conclusions and future directions are presented in Sec. V.

II. Linear Parameter-Varying Aeroservoelastic Models

Parameter-dependent linear systems are systems whose state–space descriptions are known functions of time-varying parameters. Linear, parameter-varying systems were introduced in the context of gain scheduling [18]. Since then, the LPV framework has been widely used to design controllers for nonlinear systems, including aerospace systems [19–24,33–35].

LPV systems are described by the state–space realization:

$$\begin{bmatrix} \dot{x}(t) \\ y(t) \end{bmatrix} = \begin{bmatrix} A(\rho(t)) & B(\rho(t)) \\ C(\rho(t)) & D(\rho(t)) \end{bmatrix} \begin{bmatrix} x(t) \\ u(t) \end{bmatrix} \tag{1}$$

where $x(t) \in \mathbb{R}^n$ is a collection of state variables for which the dynamic evolution is understood, $\rho(t) \in \mathbb{R}^s$ is a scheduled variable denoting exogenous parameters, $u(t) \in \mathbb{R}^m$ is the control input, and $y(t) \in \mathbb{R}^p$ is the output measurement. $A(\rho(t))$ is the state matrix, $B(\rho(t))$ is the input matrix, $C(\rho(t))$ is the output state matrix, and $D(\rho(t))$ is the input feedthrough matrix. The state–space matrices are assumed to be continuous functions of the parameter vector $\rho(t)$. The exogenous vector $\rho(t)$, contains the variables whose behavior drives the system dynamics and is measurable by sensors in real time [7]. The time variation of each of the parameters in $\rho(t)$ is not known in advance but is assumed to be bounded in magnitudes and rates by the sets $\rho_{\min}(t) \le \rho(t) \le \rho_{\max}(t)$ and $\dot{\rho}_{\min}(t) \le \dot{\rho}(t) \le \dot{\rho}_{\max}(t)$, respectively. These assumptions define a family of allowable trajectories and ensure that trajectories of the nonlinear system are also trajectories of the LPV system. For aircraft, it is often the case that the plant model varies as a function of a system state (e.g., velocity, altitude, dynamic pressure). An LPV system whose scheduled variable $\rho(t)$ is a system state is known as a quasi-LPV system [7,36].

Modeling of ASE systems requires a geometric structural model coupled with a consistent aerodynamic model. These models are usually derived using finite elements of the aircraft and panel methods for the unsteady force calculation that often depends on dynamic pressure and Mach number; thus, algorithms to find a flutter solution are required. Several methods for modal flutter analysis have been developed and are based on the form of the motion response assumed to solve the aeroelastic equations. The V–g method assumes sinusoidal motion of both aerodynamics and structure, while the P and P–K method assumes damped motion [10,15,37]. However, the structure of these equations does not change with the flight condition, but the coefficient values change as the flight condition changes in time. Because the traditional description of ASE models depends on flight condition, the LPV framework is convenient for representing the nonlinear dependence on parameters of these systems.

The LPV ASE models are generated with the structural dynamics matrices, generalized mass, stiffness and damping, and a linear approximation of the unsteady aerodynamics matrices with a rational matrix function in the frequency domain [10,38]. This rational approximation takes into account the delays between the displacement motion and the development of lift. However, the linear approximation results in aerodynamic lags being added as state vector components, increasing the order of the model. Hence, the state vector and input vector in ASE models are defined as

$$x(t) = \begin{bmatrix} \xi(t) \\ \dot{\xi}(t) \\ x_a(t) \end{bmatrix}, \qquad u(t) = \begin{bmatrix} \delta(t) \\ \dot{\delta}(t) \\ \ddot{\delta}(t) \end{bmatrix} \tag{2}$$

where $\xi(t)$ is the vector of generalized displacements, $\dot{\xi}(t)$ is the vector of generalized velocities, and $x_a(t)$ is the vector of aerodynamic lag states resulting from the rational function approximation. $\delta(t)$ is the vector of control-surface deflection commands with $\dot{\delta}(t)$ and $\ddot{\delta}(t)$ their velocities and accelerations accordingly. The system output vector $y(t)$ may include structural displacements, velocities, and accelerations.

Because flutter is a function of the dynamic pressure and Mach number, these variables are usually taken to be the scheduled variables $\rho(t)$. However, the dynamic pressure linearly affects the aircraft dynamics at a constant Mach condition, and so computing the dynamic pressure that causes flutter for a set of discrete Mach values will generate an accurate description of the flutter dynamics. Note that the time-dependency notation is dropped from the subsequent equations.

III. Model Order Reduction for Linear Parameter-Varying Systems

The objective of model order reduction for LPV systems is to reduce the complexity of models while preserving their state characteristics and input–output behavior. The main idea is to eliminate states with small contribution to the energy transferred from the inputs to the outputs in the frequency range of interest. A standard linear model-reduction problem is stated as follows [39]. Given a full nth-order model $G(s)$, find a lower rth-order model $G_r(s)$ such that the $\mathcal{L}_\infty$ norm of the difference between G and G_r is small. $\mathcal{L}_\infty$ defines the set of rational functions that have no poles on the imaginary axis, with the following norm:

$$\|G\|_\infty = \sup_{\omega \in \Re} \bar{\sigma}[G(j\omega)] \tag{3}$$

Equation (3) defines the $\mathcal{L}_\infty$ norm as the peak of the system transfer function magnitude. However, the $\mathcal{L}_\infty$ norm can be also interpretated in the time domain as the worst-case gain for sinusoidal inputs at any frequency. If $z(\omega)$ is the linear response of the system to a sinusoidal input $v(\omega)$, then at a given frequency ω, the gain depends on the direction of the input, and the worst-case direction is given by the maximum singular value:

$$\bar{\sigma}[G(j\omega)] = \max_{v(\omega)\neq 0} \frac{\|z(\omega)\|_2}{\|v(\omega)\|_2} \tag{4}$$

Note that the requirement on the approximation accuracy at one frequency range can be drastically different from the requirement for

another frequency range in ASE models. Because a specific frequency range is often desired, the model reduction for ASE systems can be reformulated as a frequency-weighted problem:

$$\min_{\deg(G_r)\le r} \|W_i(s)(G - G_r)W_o(s)\|_\infty \tag{5}$$

with appropiate choice of the input weighting matrix $W_i(s)$ and output weighting matrix $W_o(s)$ to weight the frequency of interest.

The model-reduction problem stated in Eq. (5) has been widely studied for linear time-invariant (LTI) systems, and several methods have been proposed over the years. However, this paper uses an LPV model to represent the dynamics of ASE systems. To address the LPV model-reduction problem, traditional model-reduction techniques for LTI systems have been extended to LPV systems [25–30]. Most of these methods use particular realizations that show interesting properties of the system and make it convenient for model-reduction purposes. In general, several realizations can be obtained for a particular system. These realizations are usually found by using similarity transformations that preserve the properties of the system. Given the state–space system in Eq. (1), there exists a nonsigular transformation $T(\rho)$ such that, for fixed value of the parameter ρ,

$$\begin{bmatrix} \dot{\bar{x}} \\ y \end{bmatrix} = \begin{bmatrix} \bar{A}(\rho) & \bar{B}(\rho) \\ \bar{C}(\rho) & \bar{D}(\rho) \end{bmatrix} \begin{bmatrix} \bar{x} \\ u \end{bmatrix} = \begin{bmatrix} T(\rho)A(\rho)T^{-1}(\rho) & T(\rho)B(\rho) \\ C(\rho)T^{-1}(\rho) & D(\rho) \end{bmatrix} \begin{bmatrix} \bar{x} \\ u \end{bmatrix} \tag{6}$$

Equation (6) shows the transformed realization for a fixed parameter ρ. This means that, for each value of ρ, there exists a state transformation matrix $T(\rho)$; hence, a set of different states is created at each operation point. A consistent set of states for all the parameters ρ is required for the reduced-order LPV model.

By allowing the parameter to be time-varying, derivatives of the transformation matrix are introduced to find a consistent state vector for all the parameters ρ. Thus, there exists a differentiable transformation $T(\rho)$ such that an LPV realization is computed as

$$\begin{bmatrix} \dot{\bar{x}} \\ y \end{bmatrix} = \begin{bmatrix} \bar{A}(\rho) & \bar{B}(\rho) \\ \bar{C}(\rho) & \bar{D}(\rho) \end{bmatrix} \begin{bmatrix} \bar{x} \\ u \end{bmatrix} = \begin{bmatrix} [T(\rho)A(\rho) + \frac{\partial T}{\partial \rho}\dot{\rho}]T^{-1}(\rho) & T(\rho)B(\rho) \\ C(\rho)T^{-1}(\rho) & D(\rho) \end{bmatrix} \begin{bmatrix} \bar{x} \\ u \end{bmatrix} \tag{7}$$

However, introducing a parameter-dependent transformation changes the model with dependence only on ρ to a model that depends on ρ and $\dot{\rho}$, increasing the complexity of the LPV model and the computational limitations of the LPV model-reduction problem. Hence, a time-invariant transformation that generates an LPV realization with consistent states for all of the feasible parameters is desired.

Model-reduction techniques often require stability of the system. Because ASE models have mixed stability (i.e., at some parameter values, the LTI realization is unstable), the need to extend these methods to deal with unstable LPV systems is evident. This paper focuses on the LPV model-reduction techniques that require only LTI transformations and can handle mixed stability problems.

Four model-reduction techniques for LPV ASE systems are described in the following subsections. Note that the nth state–space model in Eq. (1) is partitioned as

$$\begin{aligned} \dot{x}_1 &= A_{11}(\rho)x_1 + A_{12}(\rho)x_2 + B_1(\rho)u \\ \dot{x}_2 &= A_{21}(\rho)x_1 + A_{22}(\rho)x_2 + B_2(\rho)u \\ y &= C_1(\rho)x_1 + C_2(\rho)x_2 + D(\rho)u \end{aligned} \tag{8}$$

where x_1 is the vector of r states to preserve, and x_2 contains the $n - r$ states to remove. This notation is used to describe the different model-reduction techniques presented in the following sections.

A. Truncation

Model reduction by truncation is preferred when accuracy of the reduced-order model at high frequencies is required. The truncated model G_r is equal to the full-order model G at infinity frequency, $G(\infty) = G_r(\infty) = D(\rho)$, and it is obtained by eliminating the states in the vector x_2 [40]. Hence, the truncated model G_r is equivalent to

$$\dot{x}_1 = A_{11}(\rho)x_1 + B_1(\rho)u, \quad y = C_1(\rho)x_1 + D(\rho)u \tag{9}$$

B. Residualization

Residualization preserves the steady-state gain of the system, $G(0) = G_r(0)$, by setting the state derivatives to zero. Hence, residualization retains the accuracy of the reduced-order model at low frequency [40]. The solution for the residualized model G_r is given by

$$\begin{aligned} \dot{x}_1 &= (A_{11}(\rho) - A_{12}(\rho)A_{22}(\rho)^{-1}A_{21}(\rho))x_1 \\ &\quad + (B_1(\rho) - A_{12(\rho)}A_{22}(\rho)^{-1}B_2(\rho))u \\ y &= (C_1(\rho) - C_2(\rho)A_{22}(\rho)^{-1}A_{21}(\rho))x_1 \\ &\quad + (D(\rho) - C_2(\rho)A_{22}(\rho)^{-1}B_2(\rho))u \end{aligned} \tag{10}$$

C. Modal Reduction

Elimination of structural modes has been used with success on models of flexible structures. Consider a system described as the contribution of individual vibration modes. For a fixed value of the parameter γ, there exists a state transformation matrix $T(\gamma)$ such that the state matrix $\bar{A}(\gamma)$ in Eq. (6) is in diagonal form so that

$$\bar{A}(\gamma) = \begin{bmatrix} \lambda_1(\gamma) & & & \\ & \lambda_2(\gamma) & & \\ & & \ddots & \\ & & & \lambda_n(\gamma) \end{bmatrix} \tag{11}$$

and the matrices $\bar{B}(\gamma)$ and $\bar{C}(\gamma)$ are partioned as

$$\bar{B}(\gamma) = \begin{bmatrix} \bar{B}_1(\gamma) \\ \bar{B}_2(\gamma) \\ \vdots \\ \bar{B}_n(\gamma) \end{bmatrix}, \qquad \bar{C}(\gamma) = [\,\bar{C}_1(\gamma) \quad \bar{C}_2(\gamma) \quad \cdots \quad \bar{C}_n(\gamma)\,] \tag{12}$$

The reduced model retains only the states in the frequency range of interest. Partitioning the state matrix $\bar{A}(\gamma) = \mathrm{diag}(\bar{A}_r(\gamma), \bar{A}_{n-r}(\gamma))$, where $\bar{A}_r(\gamma)$ contains the r modes to retain and $\bar{A}_{n-r}(\gamma)$ the modes to remove, the reduced model is such that

$$\dot{\bar{x}}_r = \bar{A}_r(\gamma)\bar{x}_r + \bar{B}_r(\gamma)u, \quad y = \bar{C}_r(\gamma)\bar{x}_r + D(\gamma)u \tag{13}$$

where $\bar{x}_r$ is the modal vector of r states to preserve.

D. Balanced Reduction

Balanced model reduction is based on the measure of the controllability and observability of the state–space model. These measures are given by the controllability and observability Gramians defined for a fixed parameter value, respectively, as

$$P(\gamma) = \int_0^\infty e^{A(\gamma)t}B(\gamma)B^T(\gamma)e^{A^T(\gamma)t}\,\mathrm{d}t \tag{14}$$

$$Q(\gamma) = \int_0^\infty e^{A^T(\gamma)t}C^T(\gamma)C(\gamma)e^{A(\gamma)t}\,\mathrm{d}t \tag{15}$$

Solutions to these integrals are also the solutions to the following Lyapunov equations [39]:

$$A(\gamma)P(\gamma) + P(\gamma)A^T(\gamma) + B(\gamma)B^T(\gamma) = 0 \tag{16}$$

$$A^T(\gamma)Q(\gamma) + Q(\gamma)A(\gamma) + C^T(\gamma)C(\gamma) = 0 \tag{17}$$

Unfortunately, the controllability and observability Gramians given by Eqs. (14) and (15) are not defined for unstable systems because the integrals will be unbounded if the matrix $A(\gamma)$ is not Hurwitz (i.e., stable). The standard balanced reduction approaches require the nominal system to be stable. Because ASE models are mixed stability systems, a balanced model-reduction technique that handles stable and unstable modes in the same framework is required. Hence, a coprime factorization approach proposed in the literature to find the controllability and observability Gramians and a balanced reduced model for mixed stability systems is considered.

Defining as G_ρ the realization given by Eq. (1), there is a contractive right coprime factorization $G_\rho = N_\rho M_\rho^{-1}$ such that set of all stable input–output pairs is given by

$$\begin{bmatrix} y \\ u \end{bmatrix} = \begin{bmatrix} N_\rho \\ M_\rho \end{bmatrix} q \tag{18}$$

where q is square integrable over the infinite time axis [28,29]. A realization for this contractive right coprime factorization is defined as

$$\begin{bmatrix} \dot{x} \\ y \\ u \end{bmatrix} = \begin{bmatrix} A(\rho) + B(\rho)F(\rho) & B(\rho)S^{-1/2}(\rho) \\ C(\rho) + D(\rho)F(\rho) & D(\rho)S^{-1/2}(\rho) \\ F(\rho) & S^{-1/2}(\rho) \end{bmatrix} \begin{bmatrix} x \\ q \end{bmatrix} \tag{19}$$

where $S(\rho) = I + D^T(\rho)D(\rho)$, $F(\rho) = -S(\rho)^{-1}(B^T(\rho)X + D^T(\rho)C(\rho))$, and $X = X^T > 0$ is a constant solution of the generalized control Ricatti inequality (GCRI):

$$\begin{aligned}(A(\rho) - B(\rho)S^{-1}(\rho)D^T(\rho)C(\rho))^T X + X(A(\rho) \\ - B(\rho)S^{-1}(\rho)D^T(\rho)C(\rho)) \\ - XB(\rho)S^{-1}(\rho)B^T(\rho)X + C^T(\rho)R^{-1}(\rho)C(\rho) < 0\end{aligned} \tag{20}$$

with $R(\rho) = I + D(\rho)D^T(\rho)$.

The controllability Gramian P and observability Gramian Q of the contractive right coprime factorization are given by

$$Q = X \tag{21}$$

$$P = (I + YX)^{-1}Y \tag{22}$$

where X solves the GCRI, and $Y = Y^T > 0$ solves the generalized filtering Riccati inequality (GFRI) defined as

$$\begin{aligned}(A(\rho) - B(\rho)D^T(\rho)R^{-1}(\rho)C(\rho))Y \\ + Y(A(\rho) - B(\rho)D^T(\rho)R^{-1}(\rho)C(\rho))^T \\ - YC^T(\rho)R^{-1}(\rho)C(\rho)Y + B(\rho)S^{-1}(\rho)B^T(\rho) < 0\end{aligned} \tag{23}$$

Solutions for these Riccati Inequalities are the solutions for the linear matrix inequalities obtained by changing the variables $\bar{X} = X^{-1}$, $\bar{Y} = Y^{-1}$, and applying the Schur complement lemma:

$$\begin{bmatrix} \bar{X}A_C^T(\rho) + A_C(\rho)\bar{X} - B(\rho)S^{-1}(\rho)B^T(\rho) & \bar{X}C^T(\rho) \\ C(\rho)\bar{X} & -R(\rho) \end{bmatrix} < 0 \tag{24}$$

$$\begin{bmatrix} \bar{Y}A_F(\rho) + A_F^T(\rho)\bar{Y} - C^T(\rho)R^{-1}(\rho)C(\rho) & \bar{Y}B(\rho) \\ B^T(\rho)\bar{Y} & -S(\rho) \end{bmatrix} < 0 \tag{25}$$

where $A_C(\rho) = A(\rho) - B(\rho)S^{-1}(\rho)D^T(\rho)C(\rho)$, and $A_F(\rho) = A(\rho) - B(\rho)D^T(\rho)R^{-1}(\rho)C(\rho)$.

A balanced realization of a system is a realization with equal, diagonal controllability and observability Gramians, $\hat{P} = \hat{Q} = \Sigma$. Here, Σ is denoted as the Hankel singular values matrix. The balancing state transformation T is constant and chosen such that $\hat{P} = TPT^T$ and $\hat{Q} = (T^{-1})^T QT^{-1}$. Note also that $\hat{P}\,\hat{Q} = TPQT^{-1}$; therefore, the transformation T leads to an eigenvector decomposition $PQ = T^{-1}\Lambda T$ with $\Lambda = \mathrm{diag}(\lambda_1, \ldots, \lambda_n)$.

The balanced parameter-varying coprime factorization of G_ρ is

$$\begin{bmatrix} \dot{\bar{x}} \\ y \\ u \end{bmatrix} = \begin{bmatrix} \bar{A}(\rho) + \bar{B}(\rho)\bar{F}(\rho) & \bar{B}(\rho)S^{-1/2}(\rho) \\ \bar{C}(\rho) + D(\rho)\bar{F}(\rho) & D(\rho)S^{-1/2}(\rho) \\ \bar{F}(\rho) & S^{-1/2}(\rho) \end{bmatrix} \begin{bmatrix} \bar{x} \\ q \end{bmatrix} \tag{26}$$

where $\bar{A}(\rho) = T^{-1}A(\rho)T$, $\bar{B}(\rho) = T^{-1}B(\rho)$, $\bar{C}(\rho) = C(\rho)T$, $\bar{F}(\rho) = -S^{-1}(\rho)(\bar{B}^T(\rho)\Sigma + D^T\bar{C}(\rho))$, and q is the set of all stable input signals. The realization obtained reflects the combined controllability and observability of the individual states. Small singular values of controllability and observability Gramians indicate that a finite amount of energy in a given input do not result in significant energy in the output; hence, those states can be deleted while retaining the important input–output characteristics of the system.

The system in Eq. (26) is partitioned such that $\Sigma = \mathrm{diag}(\Sigma_1, \Sigma_2)$, where Σ_1 is related with the most controllable and observable states, and Σ_2 is related with the least controllable and observable directions. Residualizing the states corresponding to Σ_2, the reduced rth model $G_{\rho_r} = N_{\rho_r} M_{\rho_r}^{-1}$ is expressed as follows:

$$\begin{bmatrix} \dot{\bar{x}}_r \\ y \end{bmatrix} = \begin{bmatrix} A_s(\rho) - B_s(\rho)D_{ms}^{-1}(\rho)C_{ms}(\rho) & B_s(\rho)D_{ms}^{-1}(\rho) \\ C_{ns}(\rho) - D_{ns}(\rho)D_{ms}^{-1}(\rho)C_{ms}(\rho) & D_{ns}(\rho)D_{ms}^{-1}(\rho) \end{bmatrix} \begin{bmatrix} \bar{x}_r \\ u \end{bmatrix} \tag{27}$$

where

$$\begin{aligned}
A_s(\rho) &= \bar{A}_{11}(\rho) + \bar{B}_1(\rho)\bar{F}_1(\rho) - (\bar{A}_{12} + \bar{B}_1(\rho)\bar{F}_2(\rho)) \\
&\quad \times (\bar{A}_{22} + \bar{B}_2(\rho)\bar{F}_2(\rho))^{-1}(\bar{A}_{21} + \bar{B}_2(\rho)\bar{F}_1(\rho)) \\
B_s(\rho) &= \bar{B}_1(\rho)S^{-1/2}(\rho) - (\bar{A}_{12} + \bar{B}_1(\rho)\bar{F}_2(\rho)) \\
&\quad \times (\bar{A}_{22} + \bar{B}_2(\rho)\bar{F}_2(\rho))^{-1}(\bar{B}_2 S^{-1/2}(\rho)) \\
C_{ns}(\rho) &= \bar{C}_1(\rho) + D(\rho)\bar{F}_1(\rho) - (\bar{C}_2 + D(\rho)\bar{F}_2(\rho)) \\
&\quad \times (\bar{A}_{22} + \bar{B}_2(\rho)\bar{F}_2(\rho))^{-1}(\bar{A}_{21} + \bar{B}_2(\rho)\bar{F}_1(\rho)) \\
C_{ms}(\rho) &= \bar{F}_1(\rho) - \bar{F}_2(\bar{A}_{22} + \bar{B}_2(\rho)\bar{F}_2(\rho))^{-1}(\bar{A}_{21} + \bar{B}_2(\rho)\bar{F}_1(\rho)) \\
D_{ns}(\rho) &= D(\rho)S^{-1/2}(\rho) - (\bar{C}_2 + D(\rho)\bar{F}_2(\rho)) \\
&\quad \times (\bar{A}_{22} + \bar{B}_2(\rho)\bar{F}_2(\rho))^{-1}(\bar{B}_2 S^{-1/2}(\rho)) \\
D_{ms}(\rho) &= S^{-1/2}(\rho) - \bar{F}_2(\bar{A}_{22} + \bar{B}_2(\rho)\bar{F}_2(\rho))^{-1}(\bar{B}_2 S^{-1/2}(\rho))
\end{aligned}$$

with $\bar{A}_{11} \in \mathbb{R}^{r\times r}, \bar{A}_{12} \in \mathbb{R}^{r\times(n-r)}, \bar{A}_{21} \in \mathbb{R}^{(n-r)\times r}, \bar{A}_{22} \in \mathbb{R}^{(n-r)\times(n-r)}$, $\bar{B}_1 \in \mathbb{R}^{r\times m}$, $\bar{B}_2 \in \mathbb{R}^{(n-r)\times m}$, $\bar{C}_1 \in \mathbb{R}^{p\times r}, \bar{C}_2 \in \mathbb{R}^{p\times(n-r)}$, $\bar{F}_1 \in \mathbb{R}^{m\times r}$, and $\bar{F}_2 \in \mathbb{R}^{m\times(n-r)}$.

The coprime factorization approach described is used in this paper to find a balanced realization of LPV ASE models. Coprime factorizations generate the set of all stable input–output pairs of the system. Because LPV ASE models are mixed stability systems, the stable representation of the system provided by the coprime factorization is convinient for the ASE LPV model-reduction problem.

IV. Example: Body Freedom Flutter Aircraft

The U.S. Air Force Research Laboratory contracted with Lockheed Martin Aeronautics Company to develop a flight test vehicle, denoted the body freedom flutter (BFF) vehicle, for

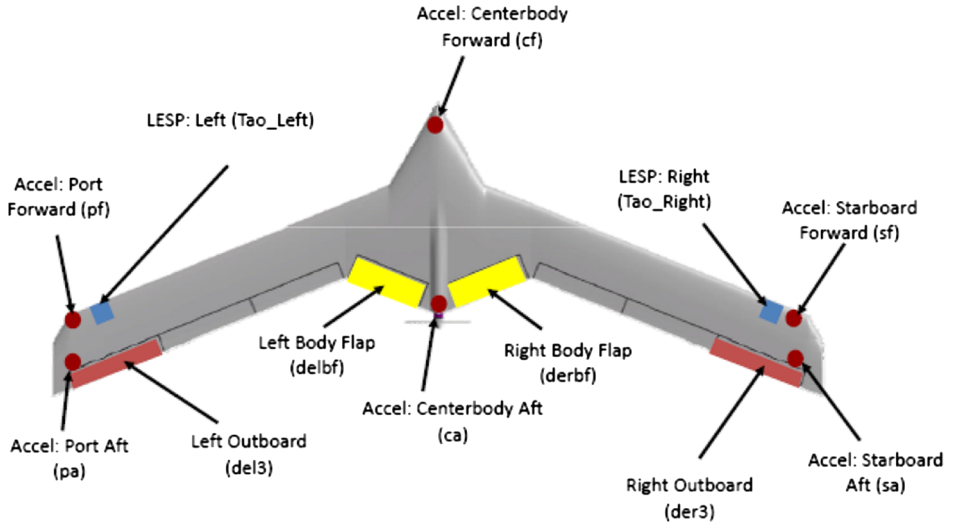

Fig. 1 Body freedom flutter vehicle [32].

demonstration of active aeroelastic control technologies [31]. The vehicle is a high-aspect-ratio flying wing with light weight airfoil. The aircraft configuration with location of accelerometers and control surfaces for flutter suppression is presented in Fig. 1.

The ASE model of the BFF vehicle was assembled using MSC/NASTRAN [15]. The initial structural model was created with 2556 degrees of freedom and reduced to 376 degrees of freedom via a Guyan reduction. A ground vibration test was performed to validate the structural model, and six critical modes were found. Table 1 lists the mode shapes and frequency values of the structural model [32]. The unsteady aerodynamics were modeled using the double lattice method in MSC/NASTRAN. A model with 2252 aerodynamic degrees of freedom was used to define accurately the aerodynamic forces of the BFF vehicle.

Linear, continuous-time, state–space models of the airframe were created using the generalized mass, stiffness, and aerodynamic force matrices generated by MSC/NASTRAN and the P–K method. A set of 26 linear models obtained at constant altitude of 1000 ft from 40 to 90 KEAS (from "knots equivalent airspeed") with increments of 2 kt describes the LPV ASE model. The full-order model has 148 states. The state vector presented in Eq. (2) consists of 37 generalized displacements $\xi(t)$, related to five rigid body modes (lateral, plunge, roll, pitch, and yaw), eight flexible modes (symmetric–antisymmetric bending and torsion), and 24 secondary discrete degrees of freedom associated with local vibration modes of the control surfaces, its derivatives $\dot{\xi}(t)$, and two aerodynamic lags for each displacement are used to approximate the rational function that describes the unsteady aerodynamics.

Bode plots of the BFF model with 148 states at three flight conditions are plotted in Fig. 2. The figure shows the dependency of the frequency response from the right outboard wing flap to the right wing accelerometer on the airspeed. The vehicle is marginally stable at 42 KEAS and has two unstable modes at 62 KEAS and three unstable modes at 90 KEAS. Figure 3 shows the frequency and damping of the critical modes of the BFF vehicle as a function of airspeed.

Table 1 Ground vibration test frequencies

Mode shape	Frequency, rad/s
Symmetric wing first bending	35.37
Antisymmetric wing first bending	54.98
Symmetric wing first torsion	123.34
Antisymmetric wing first torsion	132.76
Symmetric wing second bending	147.28
Antisymmetric wing second bending	185.73

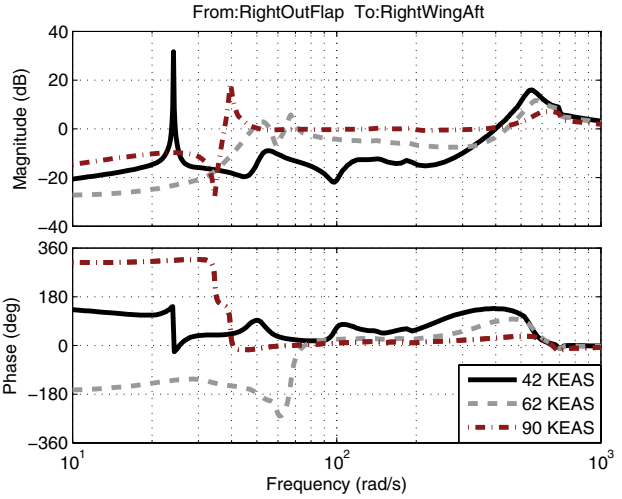

Fig. 2 Frequency response from the right outboard wing flap to the right wing accelerometer at 42, 62, and 90 KEAS.

The plots and table show how the model dynamics and system stability change dramatically as function of the airspeed. Coupling of the short period with the symmetric wing bending produces body flutter freedom at 43 KEAS with a frequency of 24.3 rad/s. Flutter is present when the symmetric wing bending and torsion modes are coupled at an airspeed of 58 KEAS with frequency of 65 rad/s. The antisymmetric wing bending and torsion modes come close in proximity at 61 KEAS with frequency of 69 rad/s, which leads to unstability. Hence, the flight envelope of the open-loop vehicle is limited to 42 KEAS before the vehicle becomes unstable.

The control objective is to extend the flight envelope of the BFF vehicle by using the selected control surfaces for flutter suppression. However, the use of an LPV ASE model with 148 states for control design is not practical; and hence a low-order LPV ASE model that captures accurately the body flutter freedom and flutter dynamics is required. Unfortunately, the abrupt change in the dynamics exhibited by the BFF vehicle is a challange for the LPV model reduction as described in the following sections.

A. Linear Parameter-Varying Model Reduction

This section presents a procedure to obtain an LPV reduced-order model that preserves the state meaning across the flight envelope. The LPV model reduction uses LTI transformations to keep a set of consistent states at all the flight conditions without increasing the complexity of the LPV model.

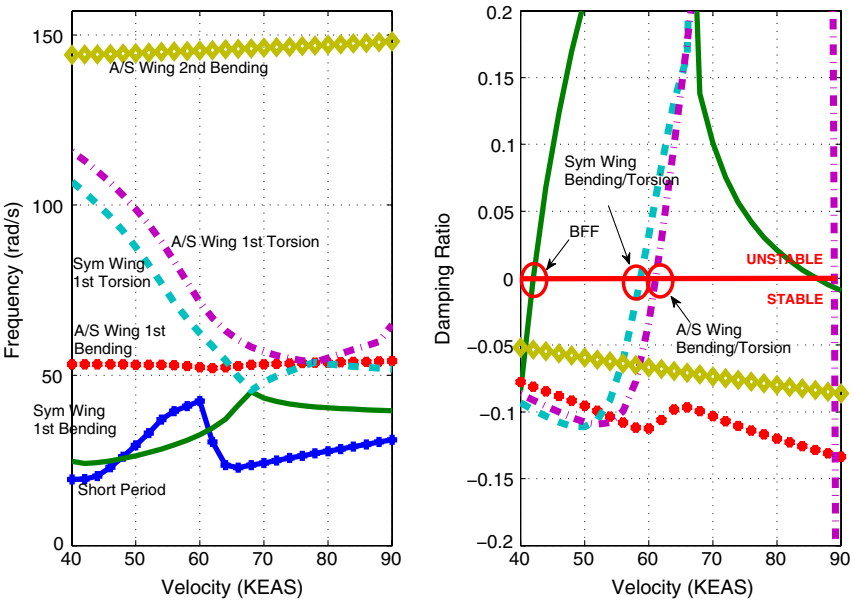

Fig. 3 Velocity/frequency/damping plot for the BFF vehicle.

The description of ASE models in the LPV system framework allows the design of nonlinear controllers using linear controller synthesis procedures. The focus of control design for the BFF vehicle is to stabilize the vehicle and actively suppress aeroelastic flutter. Hence, the LPV reduced-order model needs to capture accurately the dynamics of interest. Figure 3 shows flutter phenomena occurring between 10 and 70 rad/s across the flight envelope. However, these unstable poles impose a limitation in the control bandwidth. For stabilization and damping augmentation, the minimum bandwidth requirement is about 105 rad/s. The control surfaces actuators have a control bandwidth of 125 rad/s; thus, the frequency range of interest for the BFF model reduction is 10–125 rad/s.

The four LPV model-reduction techniques described in Sec. III are applied sequentially to the BFF vehicle. Truncation and residualization of the states are based on physical insight of the system dynamics. Balanced model reduction is performed to the coprime factor of the LPV system. Bode plots from several input/output pairs are presented to compare the approximation between the full-order model and the reduced-order model obtained.

1. *Truncation*

The goal of the model reduction by truncation is to match the response of the system at infinity frequency. Low-frequency modes outside the bandwidth of interest can be truncated from the model giving preference to high-frequency accuracy. Hence, the extremely slow dynamics of the BFF vehicle is truncated. The plunge mode, corresponding to the second state with frequency approximately four orders of magnitude below the bandwidth of interest, is eliminated from the model. Figure 4 shows the frequency response of the full-order model and the truncated model for the selected input/output pairs at two flight conditions. The plunge mode is found around 10^{-3} rad/s at all flight conditions, and it is removed in all cases because it is out of the bandwidth of interest that corresponds to 10–125 rad/s.

2. *Residualization*

Residualization of states is preferred when fidelity of the approximation at low frequencies is of interest. Modes above 125 rad/s, which corresponds to the upper bound that limits the flutter bandwidth, are residualized to obtain a lower-order model. Residualization of specific BFF states is based on the physics of the vehicle. The rigid body and flexible modes with small contribution to the vehicle response and outside the bandwidth of interest, which is delimited by solid vertical lines on the bode plots, are eliminated. The lateral, directional, symmetric wing fore-aft and antisymmetric wing second bending modes are eliminated from the LPV ASE model. In addition,

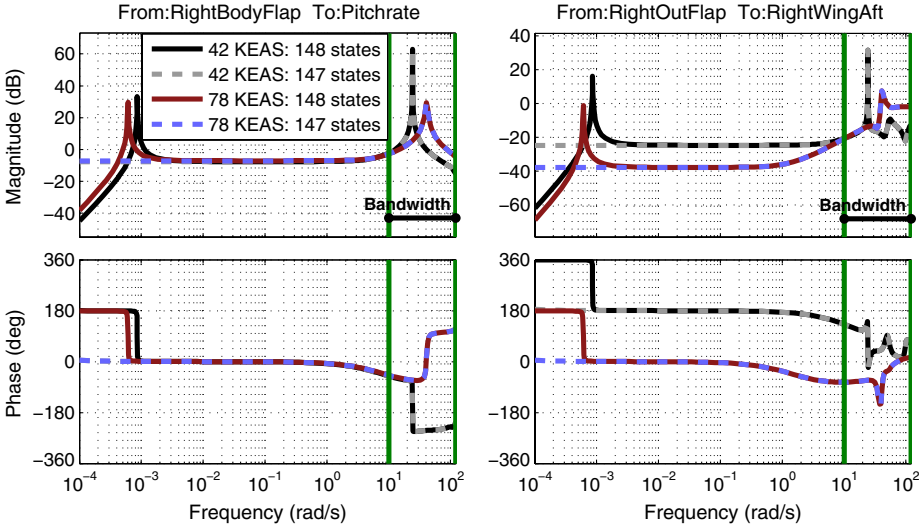

Fig. 4 Truncation: Bode plot of BFF vehicle at 42 and 78 KEAS.

rotational modes and discrete degrees of freedom corresponding to local vibration modes in the control surfaces are also found to be high-frequency modes outside the flutter bandwidth and removed from the model. In total, 92 states, two rigid body modes, three flexible modes, 18 local modes with their corresponding rates, and aerodynamic lag states associated to each mode are residualized. The resulting LPV model has 55 states. Figure 5 compares the frequency response of the truncated model obtained in the previous subsection and the model with 55 states obtained after residualization for two flight conditions. The plot shows that the residualization of these states does not affect the frequency response within the bandwidth of interest. Small changes between the reduced model and the full-order model are present above 1000 rad/s.

3. *Modal Reduction*

The Bode plots in Fig. 5 show that, after residualization of the states, high-frequency content outside the bandwidth of interest is still present in the model. These frequencies are the result of the contribution of states for which they cannot be eliminated without performing a state coordinate transformation. A constant linear transformation T, computed at 52 KEAS, is used to display the states with major contributions to the modes of the model with 55 states. This transformation is applied to all flight conditions to show that there exist six complex conjugate pair modes across the flight envelope with frequency values above the bandwidth of interest. A reduced model with 43 states is obtained by removing the 12 states out of the frequency range of interest. Figure 6 shows the frequency response of the model with 55 states and the new reduced model with 43 states for the two selected flight conditions. Notice that the reduced LPV model does not include the modes out of the flutter bandwidth, which is delimited by the solid vertical lines.

4. *Linear Parameter-Varying Coprime Factorization Model Reduction*

The objective is to find a balanced realization based on the coprime factorization of the LPV system and eliminate the least controllable and observable states. A coprime factorization of the 43 states LPV model is used to find a lower-order LPV model. The generalized controllability and observability Gramians for the LPV contractive right coprime factorization are obtained by solving the LMIs associated to the Riccati inequalities in Eqs. (24) and (25). LMI Lab in the Robust Control Toolbox for MATLAB [41] is used to find a feasible solution for this problem. The LMI problem specified for the LPV model with 43 states requires the solution of 946 decision variables subject to 27 feasibility constraints. These constraints result from the parameter gridding of the LPV system, in this case the 26 flight conditions available for the BFF model, and the positive–definite condition required for the variable matrix to solve. The solutions for the GFRI and GCRI are computed after 1 h using a standard personal computer. The generalized controllability and observability Gramians are used to find a balanced realization of the LPV coprime factorization such that the Gramians are equal and diagonal.

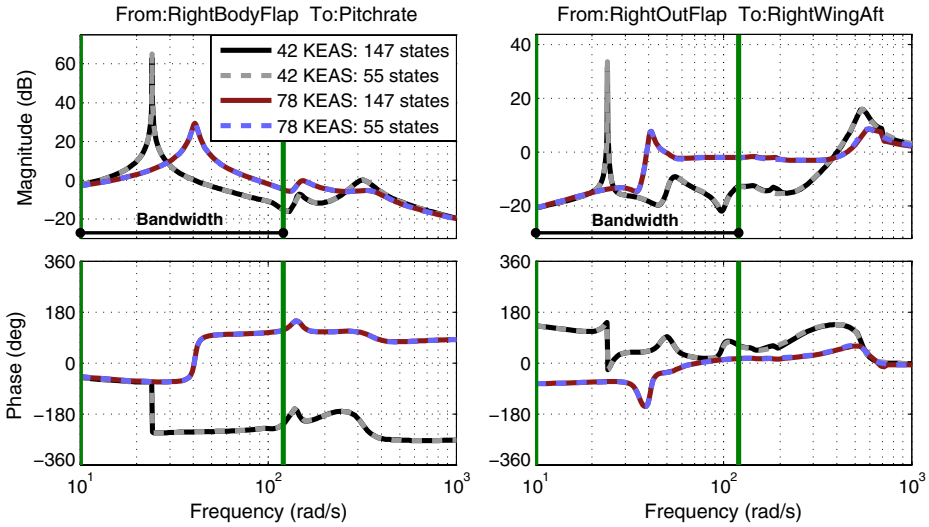

Fig. 5 Residualization: Bode plot of BFF vehicle at 42 and 78 KEAS.

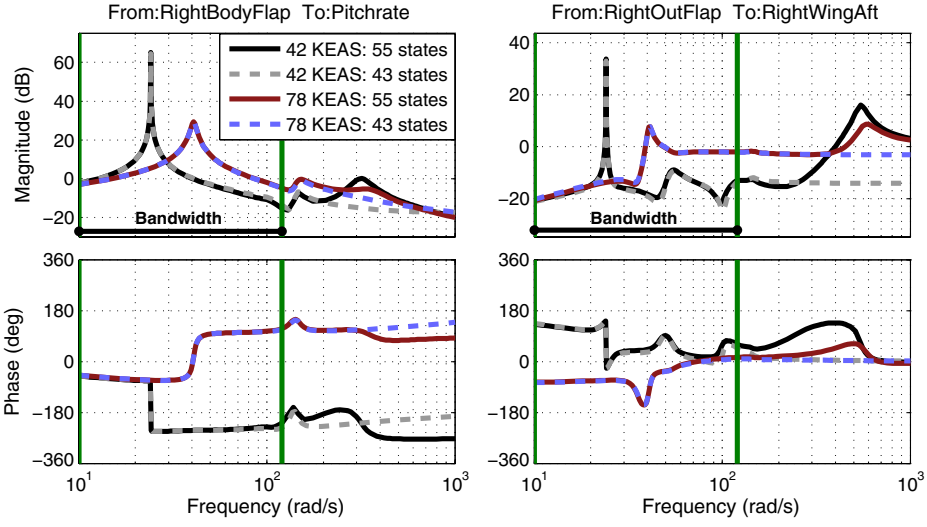

Fig. 6 Modal reduction: Bode plot of BFF vehicle at 42 and 78 KEAS.

The Hankel singular values associated with the combined controllability and observability of the system are between $1.3 \times 10^{-3} - 1.0$. A balanced low-order LPV model of the BFF vehicle is obtained by residualizing 17 states with the smallest Hankel singular values corresponding to a range of 0.0013–0.0532. The resultant LPV model has 26 states. Figure 7 compares the frequency response between the LPV model with 43 states and the balanced LPV model with 26 states for two flight conditions.

Figure 8 shows the pole location of the LPV system across the flight envelope. The plot compares the poles of the full-order model with 148 states and the balanced reduced model with 26 states obtained by the coprime factorization approach. Notice that the complex pair poles in the bandwidth of interest match accurately for all the flight conditions between 40 KEAS and 90 KEAS. The proposed approach to LPV model reduction eliminates 122 states from the BFF full-order model with 148 states.

Figure 9 compares the singular values plots between the LPV model with 43 states and the balanced LPV model with 26 states. The plots show a good approximation using the LPV model reduction based on balanced coprime factorizations. An analysis of the errors for the LPV model-reduction problem is presented in the following sections.

B. Linear Time-Invariant Model Reduction at Individual Flight Conditions

This section shows that a lower model can be obtained by treating the models at individual flight conditions as LTI systems. These results set a lower bound for the model-reduction problem for the LPV BFF vehicle. The 43 states reduced-order BFF model at 62 KEAS is chosen to perform an LTI model reduction. A coprime factorization is performed to generate the balanced reduced model of the BFF vehicle at 62 KEAS. The generalized controllability and observability Gramians are obtained by solving the equality form of the Riccati equations in Eqs. (20) and (23) at the selected flight condition.

The balanced realization of the LTI coprime factorization is obtained by computing a constant linear transformation such that the controllability and observability Gramians are equal and diagonal. In this case, the Hankel singular values of the system are between 0–0.88, and the 23 smallest Hankel singular values corresponding to the range of 0–0.0041 are eliminated from the system to obtain an LTI model with 20 states. Figure 10 compares the frequency response at 62 KEAS between the LTI model with 20 states and the LPV model with 26 states obtained in the previous section. The figure shows that the LPV reduced model with state consistency produces results comparable to the results obtained by reducing an LTI model at an individual flight condition. Because the ultimate goal is to design LPV controllers for flutter suppression, the LPV model with 26 states is more appropriated for the control synthesis.

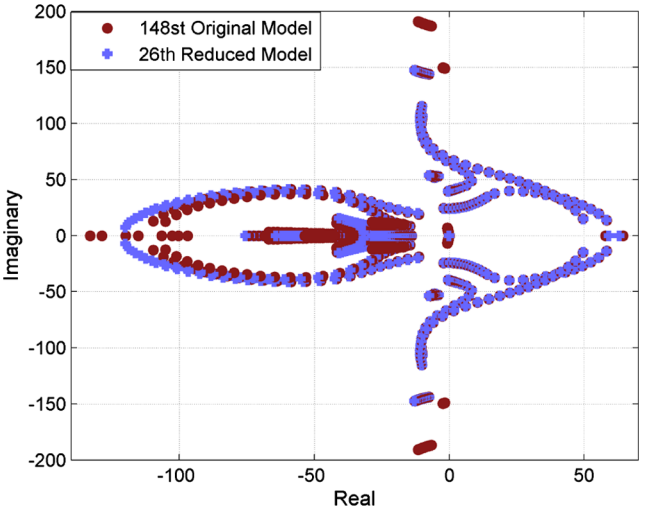

Fig. 8 Pole location of the BFF vehicle across the flight envelope.

C. Error Analysis

The model-reduction errors are calculated using the $\mathcal{L}_\infty$ criteria presented in Eq. (5) at each flight condition. Input and output weights to shape the frequency response of interest (i.e., the bandwidth of the vibration attenuation control system) are $W_i(s) = (s + 10^{-6}/s + 1)$ and $W_o(s) = (200/s + 200)$, respectively. Figure 11 shows the weighted $\mathcal{L}_\infty$ norm for the LPV model-reduction approach at each flight condition. These values correspond to differences in magnitude at flutter frequencies where the reduced model does not capture the mode damping exactly. The average approximation error between the original airframe with 148 states and the reduced model with 26 states is less than 10 dB. However, larger errors are found at flight conditions where the system is highly undamped such as 42 KEAS (see Figs. 7 and 9) and 84 KEAS. The LTI models at these flight conditions are marginally stable, with a pair of complex poles very close to the imaginary axis. Small changes in the real value of these poles lead to large differences in magnitude of the frequency response, which corresponds to the modal damping. For control purposes, capturing the frequencies accurately is more critical than capturing the damping of these modes. This implies that the model is very sensitive to any shift in frequency; thus, the changes in damping can be treated as small.

Because the $\mathcal{L}_\infty$ norm results in large errors that might not be significant for particular ASE LPV systems, a different metric to evaluate the approximation of the LPV model is desired. The ν-gap metric is useful in this case because it provides a measure of the distance between two systems in a feedback context. Two systems are

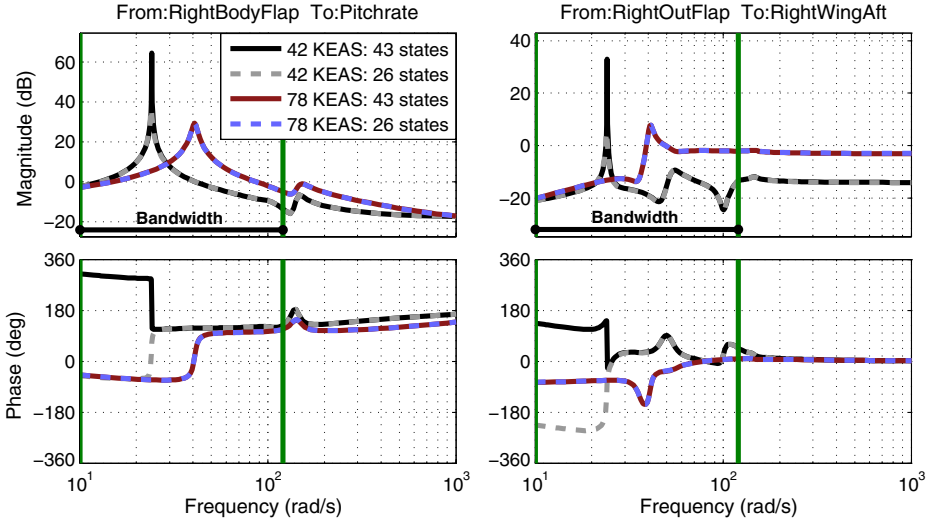

Fig. 7 LPV coprime factor reduction: Bode plot of BFF vehicle at 42 and 78 KEAS.

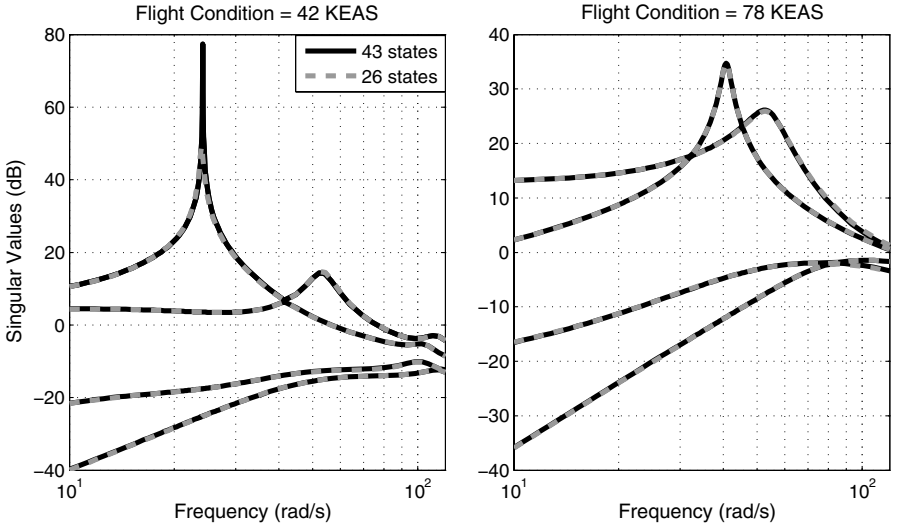

Fig. 9 LPV coprime factor reduction: singular values of the BFF vehicle at 42 and 78 KEAS.

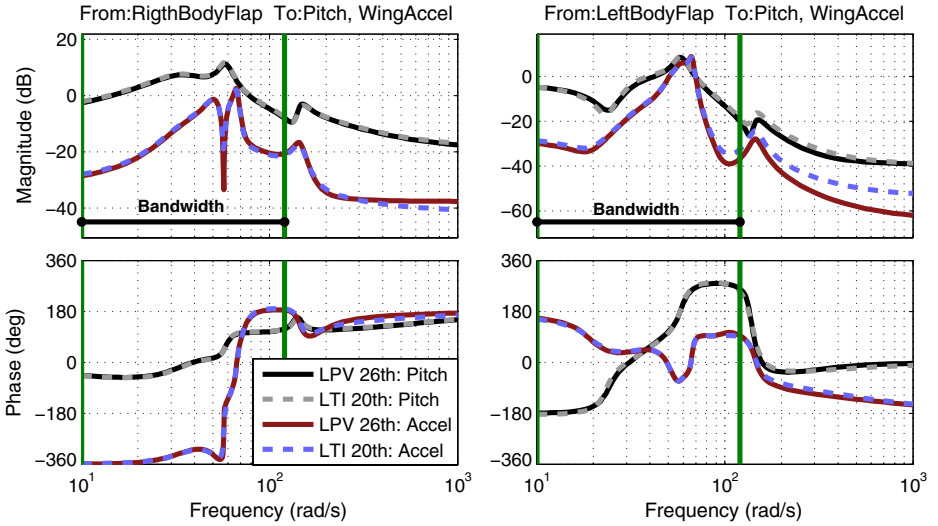

Fig. 10 LPV vs LTI coprime factor reduction: Bode plot of BFF vehicle at 62 KEAS.

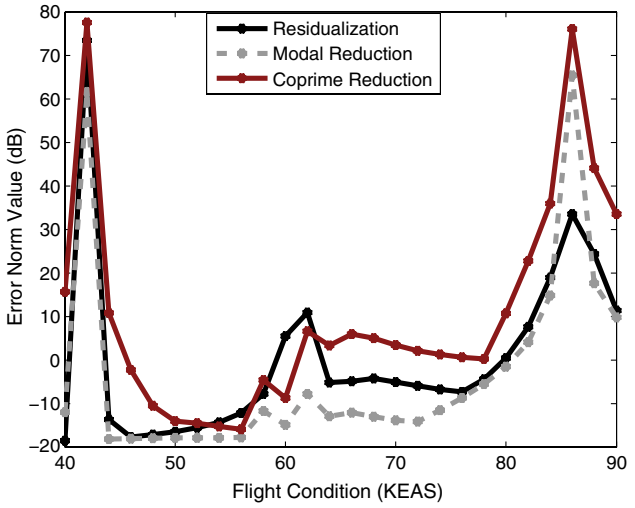

Fig. 11 LPV model reduction: approximation errors across the flight envelope.

considered to be close in the gap metric if, given any stable input–output pair of the first system, there is a corresponding stable input–output pair of the second system that is close to it [27]. The ν-gap metric $\delta_\nu(P_1, P_2)$ for two systems each with m inputs and p outputs is given by

$$\delta_\nu(P_1,P_2)=\begin{cases}\|\tilde{G}_2G_1\|_\infty & \text{if } \det(G_2^*G_1)(j\omega)\neq 0\ \forall\ \omega\in(-\infty,\infty)\\ & \text{and } wno\ \det(G_2^*G_1)=0\\ 1 & \text{otherwise}\end{cases} \tag{28}$$

where G_1 denotes the normalized right coprime factorization of P_1, $\tilde{G}_2$ denotes the normalized left coprime factorization of P_2, and wno denotes the winding number. Equation (28) indicates that the ν-gap metric lies within the interval $[0, 1]$, with 0 meaning that the two plants are identical and 1 meaning that the plants are far apart.

The ν-gap metric is computed between the original and reduced system at each flight condition [41]. Figure 12 shows the ν-gap metric distances between the original model and the LPV model with 26 states obtained by the coprime factorization approach. In addition, the distances between the original model and a LTI model with 26 states obtained at individual flight conditions are plotted in gray.

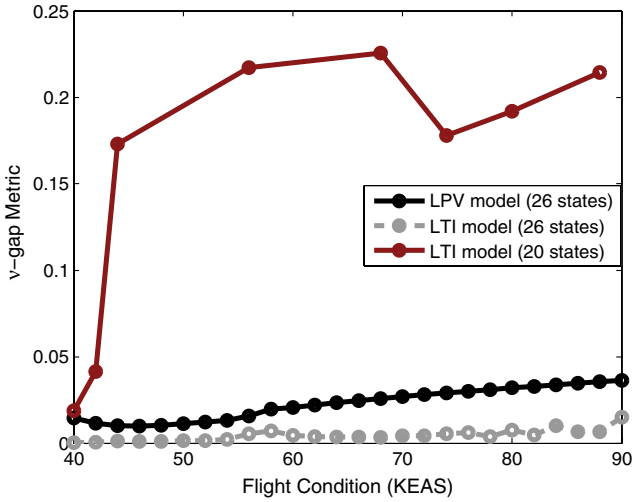

Fig. 12 Distance between original and reduced-order models for LPV and LTI cases.

Notice that the ν-gap metric values for the LTI model with 26 states are smaller than the values obtained for the LPV model across the flight envelope, as was to be expected. However, the ν-gap metric for the LTI model with 20 states obtained in the previous section result in significant higher values than the distances obtained for the LPV model with 26 states. This implies that the LPV model with 26 states obtained with the proposed approach is closer to the original model than the lower-order 20 states LTI model obtained by individual point model reduction.

The ν-gap metric compares the performance between two systems for a reasonable stabilizing controller. $\mathcal{L}_\infty$ norm values in Fig. 11 show the differences in magnitude between the two models in an open-loop configuration. Large errors are observed when lightly damped systems are evaluated. Because the control design is more sensitive to changes in frequency rather than damping, the ν-gap metric results more appropriate to measure the approximation of the LPV reduced model by comparing the two models in a closed-loop configuration.

D. Numerical Issues

LPV coprime model reduction requires the solution of the two linear matrix inequalities in Eqs. (24) and (25). The size of the LMI problem grows as function of the state order n, the number of parameters, and the parameter gridding of the LPV system. The number of decision variables k to solve for symmetric matrices is related with the state order as $k = n(n+1)/2$. In the LPV model-reduction section, the controllability and observability Gramians are solved with a 43-state LPV model. A feasible solution was obtained for this LMI problem that involves 946 decision variables and 27 feasibility constraints. Using the BFF LPV model with 55 states resulting from the residualization of states across the flight envelope, the LMI problem involves 1540 decision variables. In this case, LMI Lab could not find a numerical feasible solution, and it is noted that the computational effort required to compute a solution for this problem increases exponentially. This is an issue that is currently being investigated.

V. Conclusions

A model reduction procedure for aeroservoelastic models based on LPV balanced realizations has been proposed. The model order reduction approach is a four-step procedure. The body freedom flutter vehicle model is initially reduced by truncation and residualization techniques. A modal transformation computed for a fixed parameter value is applied to the LPV BFF model to eliminate remaining high-frequency modes outside the bandwidth of interest. Finally, a low-order, control-oriented aircraft LPV model with 26 states consistent across the flight envelope was obtained using a coprime factorization approach. The numerical issues encountered in solving the LMI problem with high state order motivate the use of classical model-reduction techniques before the coprime factorization approach. In addition, a linear model reduction at individual points in the flight envelope indicates a lower bound for the reduced-order BFF model of 20 states. The LPV reduced-order model results in a slightly higher-order model due to the varying dynamics of the vehicle across the flight envelope, though the consistency of states across the flight envelope is useful from physical insight and it ensures easily scheduling of controllers.

Acknowledgments

This work is supported by NASA Langley Research Center Small Business Innovation Research contract NNX12CF20P awarded to Systems Technology Inc. Peter Thompson is the Systems Technology Inc. principal investigator, and Walt Silva is the NASA technical monitor. This research is also supported by the NASA Small Business Technology Transfer contract NNXIICI09P as a subcontract from Tao Systems. Arun Mangalam is the principal investigator, and Martin Brenner is the NASA technical monitor. The authors also gratefully acknowledge the financial support from Zonta International through the Amelia Earhart Fellowship awarded in 2012.

References

[1] Holm-Hansen, B., Atkinson, C., Benarek, J., Burnett, E., Nicolai, L., and Youssef, H., "Envelope Expansion of a Flexible Flying Wing by Active Flutter Suppression," *Proceedings of AUVSI's Unmanned Systems North America*, Association for Unmanned Vehicle Systems International, Arlington, VA, 2010.

[2] Mukhopadhyay, V., "Flutter Suppression Control Law Design and Testing for the Active Flexible Wing," *Journal of Aircraft*, Vol. 32, No. 1, 1995, pp. 45–51. doi:10.2514/3.46682

[3] Raghavan, B., "Flight Dynamics and Control of Highly Flexible Flying Wings," Ph.D. Dissertation, Aerospace and Ocean Enginnering Dept., Virginia Polytechnic Inst. and State Univ., Blacksburg, VA, 2009.

[4] Waszak, M., "Robust Multivariable Flutter Suppression for the Benchmark Active Control Technology (BACT) Wind-Tunnel Model," *Journal of Guidance, Control, and Dynamics*, Vol. 24, No. 1, 2001, pp. 147–153.

[5] Haley, P., and Soloway, D., "Generalized Predictive Control for Active Flutter Suppression," *IEEE Control Systems*, Vol. 17, No. 4, 1997, pp. 64–70. doi:10.1109/37.608553

[6] Barker, J. M., Balas, G. J., and Blue, P. A., "Gain-Scheduled Linear Fractional Control for Active Flutter Suppression," *Journal of Guidance, Control, and Dynamics*, Vol. 22, No. 4, 1999, pp. 507–512. doi:10.2514/2.4418

[7] Balas, G. J., "Linear, Parameter-Varying Control and Its Application to Aerospace Systems," *Proceedings of the 23rd Congress of International Council of the Aeronautical Sciences*, ICAS Paper 2002-5.4.1, Toronto, ON, Canada, 2002, pp. 1–9.

[8] Van Etten, C., Balas, G. J., and Bennani, S., "Linear Parameterically Varying Integrated Flight and Structural Mode Control for a Flexible Aircraft," *AIAA Guidance, Navigation and Control Conference*, AIAA Paper 1999-4217, Aug. 1999.

[9] Patil, M. J., and Hodges, D. H., "Flight Dynamics and Control of Highly Flexible Flying-Wings," *Journal of Aircraft*, Vol. 43, No. 6, 2006, pp. 1790–1798. doi:10.2514/1.17640

[10] Lind, R., and Brenner, M., *Robust Aeroservoelastic Stability Analysis*, Springer–Verlag, London, 1999, pp. 29–64.

[11] Benani, S., Van Staveren, J. W., Beuker, B., and Meijer, J. J., "Flutter Analysis of an F-16A/B in Heavy Store Configuration," *Journal of Aircraft*, Vol. 42, No. 6, 2005, pp. 1565–1574. doi:10.2514/1.7339

[12] Lind, R., "Flutter Margins for Multimode Unstable Couplings with Associated Flutter Confidence," *Journal of Aircraft*, Vol. 46, No. 5, 2009, pp. 1563–1568. doi:10.2514/1.40328

[13] Baldelli, D. H., Zeng, J., Lind, R., and Harris, C., "Flutter-Prediction Tool for Flight-Test-Based Aeroelastic Parameter-Varying Models," *Journal of Guidance, Control and Dynamics*, Vol. 32, No. 1, 2009, pp. 158–171. doi:10.2514/1.36584

[14] Nguyen, N., and Tuzcu, I., "Flight Dynamics of Flexible Aircraft with Aeroelastic and Inertial Force Interactions," *AIAA Atmospheric Flight Mechanics Conference*, AIAA Paper 2009-6045, Aug. 2009.
[15] MSC/NASTRAN, Structural and Multidisciplinary Finite Element Analysis, Software Package, Ver. 2012, MSC Software Corp., Santa Ana, CA, 2012.
[16] FEMAP, Engineering Finite Element Analysis, Software Package, Ver. 10.3, Siemens PLM Software, Munich, Germany, 2012.
[17] ZAERO, Engineers Toolkit for Aeroelastic Solutions, Software Package, Ver. 8.5, ZONA Technology Inc., Scottsdale, AZ, 2011.
[18] Shamma, J. S., "Analysis and Design of Gain Scheduled Control Systems," Ph.D. Dissertation, Dept. of Mechanical Engineering, Massachussets Inst. of Technology, Cambridge, MA, 1988.
[19] Becker, G., "Quadratic Stability and Performance of Linear Parameter Dependent Systems," Ph.D. Dissertation, Univ. of California, Berkeley, CA, 1993.
[20] Packard, A., "Gain Scheduling via Linear Fractional Transformations," *Systems and Control Letters*, Vol. 22, No. 2, 1994, pp. 79–92. doi:10.1016/0167-6911(94)90102-3
[21] Wu, F., Yang, X. H., Packard, A., and Becker, G., "Induced L_2-Norm Control for LPV System with Bounded Parameter Variation Rates," *Proceedings of the 1995 American Control Conference*, Vol. 3, IEEE Service Center, Piscataway, NJ, 1995, pp. 2379–2383.
[22] Apkarian, P., and Gahinet, P., "A Convex Characterization of Gain-Scheduled H_∞ Controllers," *IEEE Transactions on Automatic Control*, Vol. 40, No. 5, 1995, pp. 853–864. doi:10.1109/9.384219
[23] Helmersson, A., "Methods for Robust Gain Scheduling," Ph.D. Dissertation, Dept. of Electrical Engineering, Linkoping Univ., Linkoping, Sweden, 1995.
[24] Packard, A., and Kantner, M., "Gain Scheduling the LPV Way," *Proceedings of the 35th IEEE Conference on Decision and Control*, Vol. 4, IEEE Publ., Piscataway, NJ, 1996, pp. 3938–3941.
[25] Lall, S., and Beck, C., "Error-Bounds for Balanced Model-Reduction of Linear Time-Varying Systems," *IEEE Transactions on Automatic Control*, Vol. 48, No. 6, 2003, pp. 946–956. doi:10.1109/TAC.2003.812779
[26] Saragih, R., "Model Reduction of Linear Parameter Varying Systems Based on LMIs," *Proceedings of the 2nd IMT-GT Regional Conference on Mathematics, Statistics and Applications*, Universiti Sains Malaysia, Penang, 2006.
[27] Wood, G. D., "Control of Parameter-Dependent Mechanical Systems," Ph.D. Dissertation, Aerospace and Ocean Engineering Dept., Cambridge Univ., Cambridge, England, U.K., 1995.
[28] Widowati, R., and Bambang, R. "Model Reduction of LPV Control with Bounded Parameter Variation Rates," *Proceedings of the 6th Asian Control Conference*, Asian Control Association, Korea, 2006, pp. 289–296.
[29] Wood, G. D., Goddard, P. J., and Glover, K., "Approximation of Linear Parameter-Varying Systems," *Proceedings of the 35th IEEE Confernce on Decision and Control*, Vol. 4, IEEE Publ., Piscataway, NJ, 1996, pp. 406–411.
[30] Widowati, R., Bambang, R., Sagari, R., and Nababan, S. M., "Model Reduction for Unstable LPV System Based on Coprime Factorizations and Singular Perturbation," *Proceedings of the 5th Asian Control Conference*, Vol. 2, IEEE Service Center, Piscataway, NJ, 2004, pp. 963–970.
[31] Beranek, J., Nicolai, L., Buonanno, M., Burnett, E., Atkinson, C., Holm–Hansen, B., and Flick, P., "Conceptual Design of a Multi-Utility Aeroelastic Demonstrator," *13th AIAA/ISSMO Multidisciplinary Analysis Optimization Conference*, AIAA Paper 2010-9350, Sept. 2010.
[32] Burnett, E., Atkinson, C., Beranek, J., Sibbitt, B., Holm–Hansen, B., and Nicolai, L., "NDOF Simulation Model for Flight Control Development with Flight Test Correlation," *AIAA Modeling and Simulation Technologies Conference*, AIAA Paper 2010-7780, Aug. 2010.
[33] Wu, F., Packard, A., and Balas, G., "LPV Control Design for Pitch-Axis Missile Autopilots," *Proceedings of the 34th IEEE Conference on Decision and Control*, Vol. 1, IEEE Publ., Piscataway, NJ, 1995, pp. 188–193.
[34] Balas, G., Fialho, I. J., Packard, A., Renfrow, J., and Mullaney, C., "On the Design of LPV Controllers for the F-14 Lateral-Directional Axis During Powered Approach," *Proceedings of the 1997 American Control Conference*, Vol. 1, IEEE Service Center, Piscataway, NJ, 1997, pp. 123–127.
[35] Marcos, A., and Balas, G. J., "Development of Linear, Parameter-Varying Models for Aircraft," *Journal of Guidance, Control and Dynamics*, Vol. 27, No. 2, 2004, pp. 218–228.
[36] Balas, G. J., "Linear, Parameter-Varying Control and Its Application to a Turbofan Engine," *International Journal of Robust and Nonlinear Control*, Vol. 12, No. 9, 2002, pp. 763–796. doi:10.1002/(ISSN)1099-1239
[37] Dowell, E. H., Crawley, E. F., Curtiss, H. C. Jr., Peters, D. A., Scanlan, R. H., and Sisto, F., *A Modern Course in Aeroelasticity*, 4th ed., Kluwer Academic, Dordrecht, The Netherlands, 2004, pp. 103–127.
[38] Rodden, W. P., and Johnson, E. H., "MSC/NASTRAN Aeroelastic Analysis User's Guide," MacNeal-Schwendler Corp., Santa Ana, CA, Ver. 68, 1994, pp. 26–127.
[39] Zhou, K., Doyle, J., and Glover, K., *Robust and Optimal Control*, Prentice–Hall, Upper Saddle River, NJ, 1996, pp. 97–101, 155–171.
[40] Skogestad, S., and Postlethwaite, I., *Multivariable Feedback Control: Analysis and Design*, 2nd ed., Wiley, Chichester, England, U.K., 2005, pp. 455–471.
[41] MATLAB, Language of Technical Computing, Software Package, Ver. R2012a, MathWorks, Nattick, MA, 2012.